

RESEARCH ARTICLE | FEBRUARY 17 2026

Photoelectron spectroscopy and circular dichroism of an open-shell organometallic camphor complex

Special Collection: [Modern Approaches to Chiral Sensing: electric dipole revolution and beyond](#)

Viktoria K. Brandt ; Michele Pugini ; Nikolas Kaltsoyannis ; Gustavo A. Garcia ; Ivan Powis ; Laurent Nahon ; Dominik Stemer  



Struct. Dyn. 13, 014301 (2026)

<https://doi.org/10.1063/4.0000791>



Articles You May Be Interested In

Photoelectron circular dichroism in the multiphoton ionization by short laser pulses. II. Three- and four-photon ionization of fenchone and camphor

J. Chem. Phys. (June 2018)

Determination of chiral asymmetries in the valence photoionization of camphor enantiomers by photoelectron imaging using tunable circularly polarized light

J. Chem. Phys. (September 2006)

Conformer-selective photoelectron circular dichroism: Experimental development and application to nitrogen chirality

Struct. Dyn. (November 2025)

20 February 2026 09:29:45




Structural Dynamics
Special Topics Open for Submissions

[Learn more](#)




Photoelectron spectroscopy and circular dichroism of an open-shell organometallic camphor complex

Cite as: Struct. Dyn. **13**, 014301 (2026); doi: 10.1063/4.0000791

Submitted: 3 October 2025 · Accepted: 16 January 2026 ·

Published Online: 17 February 2026



View Online



Export Citation



CrossMark

Viktoria K. Brandt,¹ Michele Pugini,¹ Nikolas Kaltsoyannis,² Gustavo A. Garcia,³ Ivan Powis,⁴ Laurent Nahon,³ and Dominik Stermer^{1,a)}

AFFILIATIONS

¹Fritz-Haber-Institut der Max-Planck-Gesellschaft, Faradayweg 4-6, 14195 Berlin, Germany

²Department of Chemistry, The University of Manchester, Oxford Road, Manchester M13 9PL, England

³Synchrotron SOLEIL, l'Orme des merisiers, Départementale 128, St. Aubin 91190, France

⁴School of Chemistry, The University of Nottingham, University Park, Nottingham NG7 2RD, England

Note: This paper is part of the Special Topic on Modern Approaches to Chiral Sensing: electric dipole revolution and beyond.

^{a)}Author to whom correspondence should be addressed: dstermer@fhi-berlin.mpg.de

ABSTRACT

We present an investigation of one-photon valence-shell photoelectron spectroscopy and photoelectron circular dichroism (PECD) for the chiral molecule (1R,4R)-3-(heptafluorobutyl)-(+)-camphor (HFC) and its europium complex Eu(III) tris[3-(heptafluorobutyl)-(1R,4R)-camphorate] (Eu-HFC₃), the latter of which constitutes the heaviest organometallic molecule for which PECD has yet been measured. We discuss the role of keto-enol tautomerism in HFC, both as a free molecule and complexed in Eu-HFC₃. PECD is a uniquely sensitive probe of molecular chirality and structure such as absolute configuration, conformation, isomerization, and substitution, and is, in principle, well suited to unambiguously resolving tautomers; however, modeling remains challenging. For small organic molecules, theory is generally capable of accounting for experimentally measured PECD asymmetries, but significantly poorer agreement is typically achieved for the case of large open-shell systems. Here, we report PECD asymmetries, ranging up to ~8% for HFC and ~7% for Eu-HFC₃, of similar magnitude to those reported previously for smaller isolated chiral molecules, indicating that PECD remains a practical experimental technique for the study of large, complicated chiral systems.

© 2026 Author(s). All article content, except where otherwise noted, is licensed under a Creative Commons Attribution (CC BY) license (<https://creativecommons.org/licenses/by/4.0/>). <https://doi.org/10.1063/4.0000791>

I. INTRODUCTION

Photoelectron spectroscopy (PES) is a powerful method for the investigation of molecular electronic structure. Nowadays, when the molecule of interest is chiral, PES can be enhanced by the complementary technique of photoelectron circular dichroism (PECD). Chiral light-matter interactions have long been leveraged to resolve the physically and chemically indistinguishable enantiomers of various chiral molecules. The differential absorption of circularly polarized light in the infrared and UV domains has proven a particularly accessible means of probing the electric and vibrational structure of chiral molecules. However, because such absorption-based circular dichroism (CD) relies on the interaction between electronic and much weaker magnetic dipole transitions, the magnitude of the observed effects tends to be low (typically 10⁻³%–10⁻¹%). In contrast, chiral asymmetry in the photoelectron angular distribution arises purely from electric-dipole interactions, and correspondingly, the measured effects

are larger (typically 0.5–10's %), even for randomly oriented molecules.^{1–3}

PECD, which manifests as a forward-backward asymmetry in the photoelectron flux emitted along the light-propagation axis in photoionization of chiral molecules by circularly polarized light, was first predicted theoretically in 1976 by Ritchie.^{4,5} The first experimental demonstrations of this effect were published in the early 2000s.^{6,7} In subsequent years, a number of exploratory PECD studies were performed on a range of terpenes, including camphor and fenchone^{8–12} as well as several smaller systems,² thereby establishing PECD as a general phenomenon in photoionization of chiral molecules. The dependence of PECD on the final photoelectron continuum states (and thus electron kinetic energy) is clear from core-level photoionization investigations, e.g., of the C 1s orbital in camphor.^{8,12} As a 1s orbital is spherical (achiral) and highly localized, PECD asymmetry measured upon photoionization of such orbitals clearly indicates that the

outgoing photoelectrons must sample the intrinsic chirality of the full molecular potential via scattering processes. Although camphor and fenchone exhibit very similar PECD in C 1s photoionization within the kinetic-energy range of 1–15 eV,^{8,12} photoionization of their highest-occupied molecular orbitals (HOMOs) reveals remarkable differences, despite the fact that in both cases, the HOMO is strongly localized on the molecule's respective carbonyl group.^{7,10,11}

This extraordinary sensitivity to minor differences in the initial state of the molecules, as well as to the molecules' overall geometry and valence electronic structure, makes PECD an attractive technique capable of providing new insights that may aid in the interpretation of complicated photoelectron spectra. Indeed, experiment and theory both clearly indicate that PECD is much more sensitive to minor changes in a molecule's geometric or electronic structure than either of the more commonly measured photoionization observables: cross section and anisotropy parameter (β).^{1,13–15}

However, despite PECD's exceptional sensitivity, its application as a practical analytical method demands reasonable agreement between theory and experiment. A major challenge for theoreticians, in turn, is the accurate description of electron continuum states, which, together with the neutral electronic ground states, are needed to determine the photoionization matrix elements that give rise to PECD.^{16–18}

For the case of small to moderately sized organic molecules without significant electron correlation, this information is generally accessible, and thus, the agreement between PECD theory and experiment is sufficient to enable the practical use of PECD, for example in the resolution of different conformers that are indistinguishable in the angle-integrated PE spectrum.^{19–22} Even for more complicated molecules, such as closed-shell organometallic complexes, agreement between theory and experiment can be nearly quantitative for well-characterized ionization channels.²³ However, for open-shell molecules (which exhibit stronger electron correlation) or for ionization channels involving deeper valence states, and therefore not well approximated by one-electron excitations, PECD remains challenging to model, and agreement with experiment has generally been poorer.^{24,25}

Improvements in modeling will require comparison to experimental data. In the case of chiral organometallic complexes, the study of which could benefit from the unique capabilities of PECD, such data remain sparse. These molecules are of broad scientific interest for both practical applications and for tests of fundamental physics. They are regularly employed as chiral catalysts and shift reagents for nuclear magnetic resonance²⁶ and as efficient emitters for circularly polarized electroluminescence.²⁷ At a more basic level, such molecules are interesting due to their capacity to filter polarized electrons via elastic scattering at levels measurable in the laboratory^{28,29} and are useful candidates for experiments seeking to quantify minuscule energetic differences between enantiomers due to parity violation.^{30,31}

Here, we report on our recent PES and PECD experiments involving gas-phase samples of (1R,4R)-3-(heptafluorobutyl)-(+)-camphor (hereafter abbreviated HFC) and its complex with europium, Eu(III) tris[3-(heptafluorobutyl)-(1R,4R)-camphorate] (hereafter Eu-HFC₃). HFC is a camphor derivative that differs from camphor via the introduction of a large, flexible, electronegative tail at the C₃ position, adjacent to the camphor carbonyl group [see Fig. 1(a)]. This β -diketone structure may also suggest the possibility of tautomeric interconversion, giving rise to an enol form in HFC [Fig. 1(b)]. To the best of our knowledge, there has been no previous

discussion of keto-enol tautomerism in HFC, although one may anticipate that any resulting changes in electron density around the oxygen atoms would carry implications for the outer valence PES. Eu-HFC₃ is composed of three HFC molecules coordinated to a central trivalent europium cation [Fig. 1(c)]. We note that Eu-HFC₃ is at present the heaviest organometallic molecule to have been probed using PECD ($m/z = 1194$) and therefore serves as a useful candidate for assessing PECD's relevance as an analytical tool to study heavy, complex molecules with multiple chiral centers.

II. METHODS

A. Experimental

All measurements were carried out at the DESIRS VUV beamline at Synchrotron SOLEIL.³² To prepare a sufficiently dense gas-phase target using HFC (respectively Eu-HFC₃), 2 ml of the liquid sample (both molecules were obtained from Santa Cruz Biochemicals and used without further treatment) was placed into a stainless steel oven, which was subsequently heated to 55 °C (respectively 195 °C). The vapor was expanded through a 100 μ m pinhole, heated to 75 °C (respectively 215 °C), with 1 bar He carrier gas. The supersonic expansion was skimmed using two skimmers with diameters of 1.5 and 2 mm. The molecular beam was perpendicularly crossed with a VUV photon beam in the center of a ²PEPICO DELICIOUS III PEPICO spectrometer coupling a velocity-map-imaging spectrometer on the electron side with a modified Wiley-McLaren 3D momentum imaging spectrometer on the ion side.³³ The mass resolution was limited due to the high deflector voltages used to refocus the heavy ions onto the detector, at approximately $m/\Delta m = 300$. Photoelectron spectroscopy was performed using circularly polarized light in the photon energy range of 9–13 eV. For PECD, measurements were made by collecting image pairs with left- and right-handed circularly polarized light, switching polarization at ~ 15 min intervals. These were combined following an established protocol to obtain symmetric and antisymmetric images for subsequent analysis.⁹ The resulting mass-selected photoelectron images were analyzed using the pBasex inversion procedure.³⁴

Within the electric-dipole approximation, the normalized photoelectron angular distribution resulting from one-photon ionization of a randomly oriented molecule by circularly polarized radiation may be described as

$$I^{(p)}(\theta) = \left[1 + b_1^{(p)} P_1(\cos \theta) + b_2^{(p)} P_2(\cos \theta) \right], \quad (1)$$

where P_n represents the n th-order Legendre polynomial.¹ For circular polarizations, θ is the angle of photoemission with respect to the vector defined by photon propagation. The index p describes the helicity of the light: $p = \pm 1$ for left-handed (right-handed) circularly polarized light

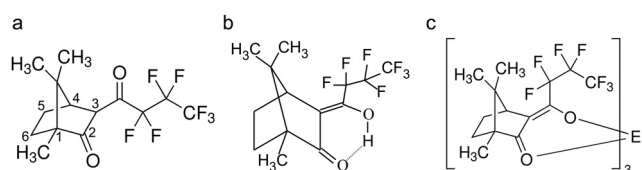


FIG. 1. Molecular structures of (1R,4R)-3-(heptafluorobutyl)-(+)-camphor (HFC) tautomers: (a) keto form; (b) enol form. The expected structure of Eu(III) tris[3-(heptafluorobutyl)-(1R,4R)-camphorate] (Eu-HFC₃) is shown in (c).

and $p = 0$ for linear polarizations. Since $P_1(\cos \theta)$ expands simply as $\cos \theta$, the chiral asymmetry parameters, $b_1^{\{\pm 1\}}$, determine the magnitude of forward-backward asymmetry. From underlying symmetry considerations, one obtains $b_1^{\{+1\}} = -b_1^{\{-1\}}$, but for linear polarizations, $b_1^{\{0\}}$ is necessarily zero. For circular polarizations, the P_2 Legendre coefficient, $b_2^{\{p\}}$, is symmetric, so that $b_2^{\{+1\}} = b_2^{\{-1\}}$, and for linear polarization, $b_2^{\{0\}} \equiv \beta$, the conventional photoelectron anisotropy parameter.

The magnitude of the measured chiral forward-backward asymmetry is generally defined as $2b_1^{\{p\}}$. In this study, we use the shorthand b_1 for $b_1^{\{+1\}}$ and PECD for $2b_1^{\{+1\}}$ when discussing derived numerical values of the chiral asymmetry.

B. Computational

Quantum chemical calculations were carried out as follows. The Gaussian 16 software package, revision C.01, was used for all density functional theory calculations.³⁵ The hybrid density functional approximation, PBE0,^{36,37} was used with Grimme's D3³⁸ and the Becke-Johnson damping parameters for dispersion corrections.^{39–41} Dunning's correlation consistent basis sets of polarized triple- ζ quality were employed for H, C, O, and F.^{42–45} A Stuttgart-Bonn relativistic effective core potential was used for Eu (28 electrons), with the associated segmented valence basis sets.^{46–48} Eu(III) has the electronic configuration [Xe]4f⁶, and hence, Eu-HFC₃ was computed as a spin-unrestricted septet. Spin contamination was minimal, with $\langle S^2 \rangle = 12.04$ for Eu-HFC₃. Default settings were used for the SCF and geometry optimizations (which were performed without symmetry constraints), and analysis of the harmonic vibrational frequencies confirmed the optimized geometries as energetic minima.

Ionization energies for the PBE0/cc-pVTZ optimized HFC geometries were calculated using the outer valence Green's function (OVGF) method⁴⁹ implemented in Gaussian 16 and the non-Dyson third-order algebraic-diagrammatic construction scheme [IP-ADC(3[4+])] implemented in Q-Chem 5.4.⁵² Both OVGF and IP-ADC(3[4+]) methods address one-hole (1h) independent-electron ionization processes through third-order many-body perturbation theory, thereby incorporating a treatment for electron correlation effects.

Neither the OVGF nor the ADC(3) calculations were feasible for the much larger Eu-HFC₃ complex. Ionization energies for this were instead estimated by the ΔE_{SCF} method, determining the energy difference between the neutral and cation states.

III. RESULTS

Representative time-of-flight (TOF) spectra obtained with the highest photon energy used for both HFC and Eu-HFC₃ (13 and 12 eV, respectively) are displayed in Figs. 2(a) and 2(c), with regions of interest highlighted in the insets. In the HFC TOF spectrum, we observed clear signatures of the parent ion at $m/z = 348$. Fragmentation of HFC is also apparent at this photon energy, revealed via the small feature at $m/z = 320$. However, in contrast to previous experiments with camphor, the parent ion remains dominant at all photon energies used,¹⁰ indicating a greater stability of HFC upon photoionization. For Eu-HFC₃, the parent ion peak at $m/z = 1194$ is also clear. In this case, we did not observe any clear signatures of fragmentation. The size of Eu-HFC₃ (339 vibrational modes) evidently constitutes a greater heat-bath capable of holding the excess energy of

ionization at the photon energies we examined, thereby stabilizing the system against fragmentation. The strong peak at $m/z = 348$ originates from unreacted ligand and is not a fragmentation product of Eu-HFC₃. This is clearly established by considering the PES obtained in coincidence with the $m/z = 348$ ions, which is identical to that for HFC. For the subsequent analysis of the PE spectra of HFC and Eu-HFC₃, we include only electrons collected in coincidence with the respective parent ion masses.

The PE spectrum of HFC [Fig. 2(b)] reveals one well-separated feature with a vertical ionization energy (VIE) of approximately 9.4 eV as well as a more complicated envelope of overlapping features beginning at slightly higher IE but with a distinct shoulder suggesting a second orbital ionization at ~ 10.5 eV. As seen in Fig. 2(b), the corresponding HFC PECD exhibits clear negative maxima centered at the IEs corresponding to these first two features in the PES. At higher ionization energy, as the apparent density of spectroscopic states increases, the PECD trends to zero.

The measured narrow valence-band spectrum of Eu-HFC₃ [Fig. 2(d)] is similar to that measured for HFC, with the notable difference being the presence of a new lower-energy feature with VIE ≈ 8.2 eV. Once again, two clear PECD extrema are seen at the IEs corresponding to the first two PE features. Similarly to HFC, we find that the higher IE features do not yield any notable PECD.

To facilitate a more direct comparison between the PECD measured for each of the above-assigned PE features for HFC and Eu-HFC₃, we averaged the PECD b_1 values across the full-width at half maximum of each peak as a function of photon energy. The summarized data are presented in Fig. 3. Beginning with the HOMO of HFC, we find clear PECD across the entire kinetic-energy range probed, with the magnitude of b_1 varying between -0.014 and -0.042. The case of the HFC HOMO-1 is quite different, with a maximum measured value of b_1 of -0.037 at 2.6 eV KE, a slight decrease in magnitude at 1.6 eV KE, and a sign reversal with $b_1 = 0.022$ for the lowest-KE electrons studied.

For Eu-HFC₃, the measured PECD magnitudes accompanying the first two PES peaks are, in general, lower, with the HOMO exhibiting a maximum magnitude for b_1 of -0.034 for 0.6 eV photoelectrons, near zero PECD for electrons with KE of 1.7 and 2.7 eV, and negative PECD once more for 3.7 eV photoelectrons. Eu-HFC₃'s HOMO-1 exhibited a maximum measured value of b_1 of -0.033 for 2.8 eV photoelectrons, with PECD magnitude decreasing for lower KE electrons. Due to time constraints, only one enantiomer of each molecule was investigated.

IV. DISCUSSION

A. HFC

Following an automated search⁵³ of the conformational space of (1R,4R)-3-heptafluorobutyl-(+)-camphor, ten potential conformers of interest reported in the PubChem database were identified.⁵⁴ Upon further examination, the heptafluorobutyl substitutions at the tetrahedrally coordinated C₃ camphor atom immediately divide into two subclasses: half occupy the endo position and another half the exo position. The C₃ atom, thus, becomes asymmetrically substituted with either R or S configurations possible, creating a second independent chiral center.⁵⁵

To aid interpretation of the photoelectron spectra, we re-optimized these ten PubChem HFC conformer structures⁵⁴ using the PBE0 hybrid functional with empirical dispersion corrections

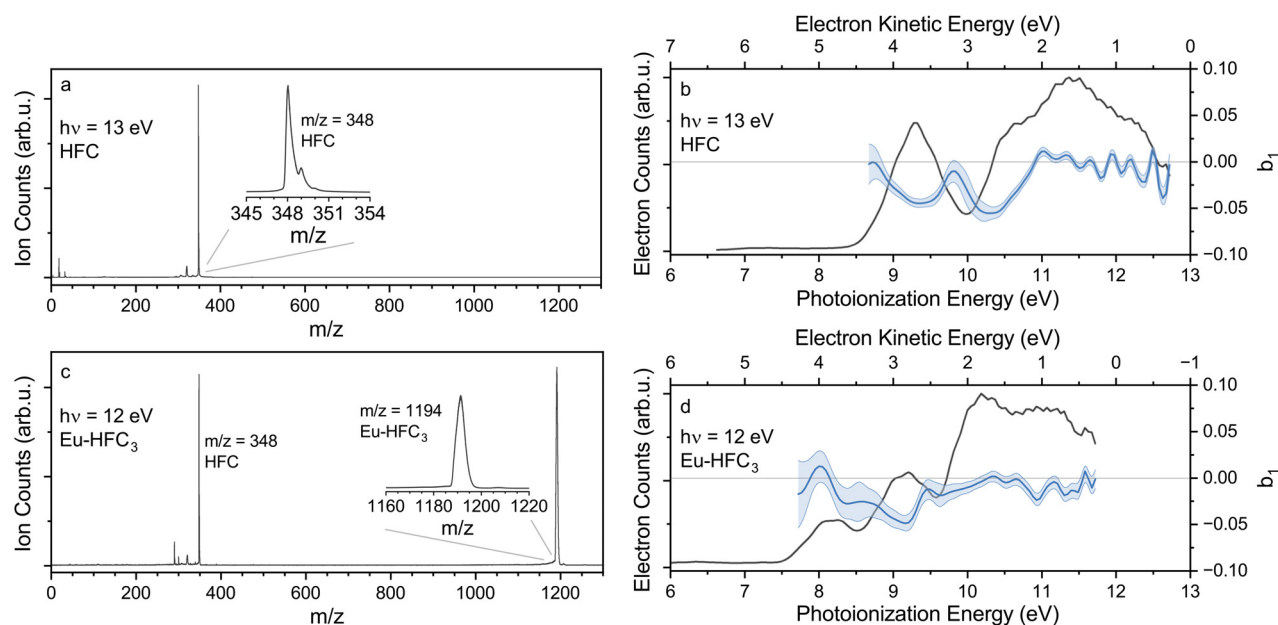


FIG. 2. Representative photoion mass time-of-flight spectra (left) and corresponding photoelectron spectra collected in coincidence with the parent ion peaks (right) for (a) and (b) HFC and (c) and (d) Eu-HFC₃. The top row HFC spectra (a) and (b) were recorded with 13 eV photon energy; the bottom row Eu(HFC)₃ (c) and (d) measurements used 12 eV photons. Expanded views of the parent ion peaks are presented in (a) and (c). Photoelectron circular dichroism traces, showing $b_1^{(+1)}$ values derived from the photoelectron velocity map images, are presented as blue traces in (b) and (d).

(as discussed in Sec. II B) to obtain more accurate SCF energies. These PBE0/cc-pVTZ results are listed in Table S1.

Apart from the endo- or exo-nature of the substitution site, these conformers differ principally in the rotamer conformations adopted in the CF₂·CF₂·CF₃ tail grouping, the bicyclic structure of the camphor moiety being relatively rigid. The estimated OVGf/cc-pVTZ ionization energies for the outermost orbitals (listed in Table S2) show very little dependence on the specific conformer structure. This invariance is perhaps not surprising as these outer orbitals localize around the more conformationally rigid camphor grouping rather than the floppier, electronegative CF₂·CF₂·CF₃ tail (Fig. S1). Indeed, the HFC valence PES [Fig. 2(b)] bears a strong similarity to that of camphor,¹¹ fenchone,¹⁰ and bromocamphor⁶ measured at comparable photon energies. For each of these molecules, the distinct HOMO band for each of these molecules may be attributed predominantly to the localized carbonyl orbital with prominent O lone-pair character. The greater VIE of the HFC HOMO compared to these other terpenes reflects the high electronegativity of the C₃ tail group.⁵⁶

The molecular structure of the lowest-computed energy conformer (keto conformer #9 in Table S1) is shown in Fig. 4(a). The OVGf ionization energies for this conformer are 9.33, 10.56, 10.76, 11.30, and 11.55 eV for the HOMO–HOMO-4, respectively. The vertical ionization energies for the HOMO and HOMO-1, in particular, are in excellent accord with the visible peak positions in the PES and PECD spectra [Fig. 2(b)]. We thus conclude that these calculations provide a convincing assignment for at least the first two distinct photoelectron bands. Although our IP-ADC(3[4+]) calculations were more limited in overall scope, these results (Table S3) are in good agreement with the OVGf results.

Each of the above-discussed HFCs structure is of the diketone form illustrated in Fig. 1, which is how HFC is generally presented in vendor catalogs and online databases. However, we note that this is neither the only possible structure nor even necessarily the most energetically stable one. In an experimental and computational vibrational circular dichroism (VCD) study of the closely related β -diketone molecule 3-(trifluoroacetyl)-camphor (TFA),⁵⁷ the possibility of keto-enol tautomerism was considered. In the enolization process, a proton migrates from the C₃ atom creating a C=C double bond at that point and an adjacent OH group, which may then H-bond toward the second C₂ = O carbonyl group, resulting in the formation of a hydroxy-ketone group [the analogous HFC enol structure is shown in Figs. 1(b) and 4(d)]. Using DFT calculations with a polarizable continuum model, the authors found that, for the case of solution-phase TFA in chloroform, the enol form of the molecule was ~ 19 kJ mol⁻¹ more stable than the keto forms. The experimental VCD spectrum matched well with that calculated for the most stable enol tautomer and differed substantially from the calculated keto spectrum, providing further evidence for the dominance of the enol form of the molecule in solution.

While these solution-phase results for TFA may not directly apply to the gas phase, they strongly recommended the consideration of additional HFC structures. As such, we have extended our calculations to include HFC enol structures. Specifically, we generated trial structures starting from the two lowest-energy keto forms (keto conformers #9 and #1 in Table S1) to define the CF₂·CF₂·CF₃ tail conformation and re-optimized with a PBE0/cc-pVTZ calculation. We found that the enol is predicted to be ~ 30 kJ mol⁻¹ more stable than the keto forms, suggesting that it would dominate any equilibrium mixture. While we have not investigated the HFC enol tail conformers as

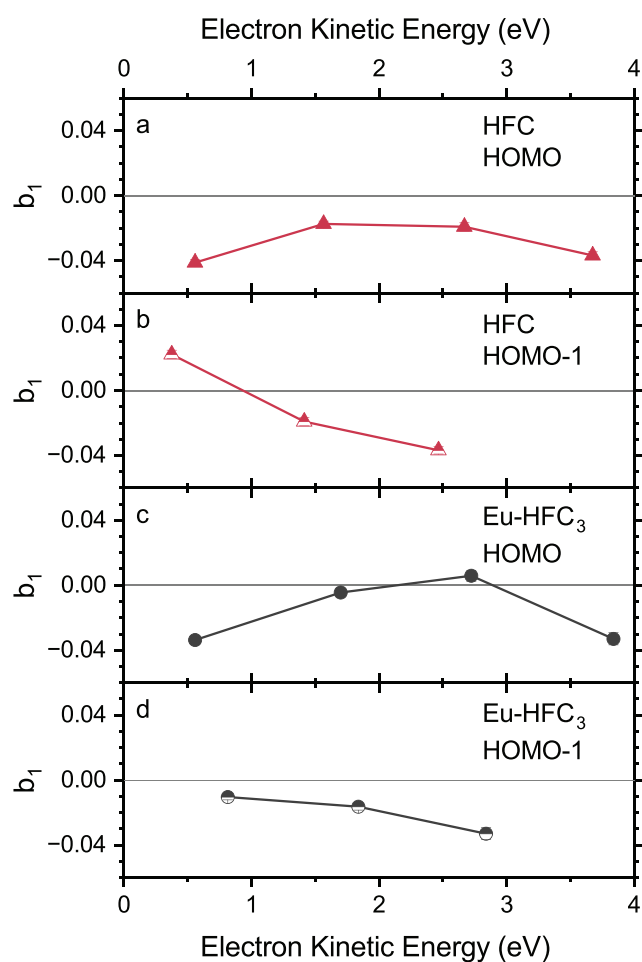


FIG. 3. Photoelectron circular dichroism measured as a function of photoelectron kinetic energy for the two highest-occupied molecular orbitals of (a) and (b) HFC and (c) and (d) Eu-HFC₃. Statistical error bars are included but are generally smaller than the markers.

extensively as was done for the keto forms, our experience with the latter suggests that this will not significantly influence the broad conclusions to be drawn.

Without solvation effects, this dramatic stabilization in the gas-phase HFC enol must be attributed to the formation of a six-membered H-bonded ring structure along with the increased conjugation in the enol [Figs. 1(b) and 4(d)]. These structural changes are correspondingly apparent in the orbitals, notably those located near the hydroxyketone group. In particular, the enol HFC HOMO spans O=C–C=C conjugation [Fig. 4(e)], while the HOMO-1 looks remarkably similar to the keto HOMO, with clear localization on the C₂ = O carbonyl group [compare Figs. 4(b) and 4(f)]. The keto HOMO-1 is heavily localized on the tail carbonyl group, Fig. 4(c). Both our OVG and ADC(3) ionization energy calculations (Tables S1 and S3) show that the VIE of the enol HOMO is strongly shifted to ~8.9 eV, approximately 0.4 eV below the keto HOMO ionization.

It is apparent that the predicted enol HOMO vertical ionization energy is in rather worse agreement with the experimental PE

spectrum [Fig. 2(b)] than the earlier keto HFC predictions. This creates a paradox since the foregoing arguments for a dominant role of the enol form seem to be in conflict with the experimental PES evidence. One may speculate that a high keto-enol interconversion energetic barrier could explain the apparent preference of the keto form in the PES data as a consequence of kinetics, in spite of the strongly favorable equilibrium energetics. Ultimately, the PECD data measured may provide an ideal means to clarify the diastereomeric character of gas-phase HFC and thereby to provide insights into the keto-enol equilibrium in this system, which are not directly accessible via the PES. However, despite the strong HFC PECD signal reported here, the use of the PECD data in this analytic capacity will require reliable, high-quality theoretical modeling, which is beyond the scope of the present study.

B. Eu-HFC₃

We optimized the structure of Eu-HFC₃ beginning with the bidentate ligand binding geometry suggested by Whitesides and Lewis.⁵⁸ The resulting structure is shown in Fig. 5(a) and implies that the coordinated HFC ligands adopt the enol form. We will examine the accuracy of this assumption shortly. We also note that this structure is nearly C₃ symmetric and, as such, may be expected to exhibit helical, or P–M, chirality. For this type of chirality, the sign of the “twist” in the ligand packing configuration distinguishes two enantiomers, even for the case when the ligands themselves are achiral. This is similar, but not identical to, the case of the D₃-symmetric Ru(acac)₃, for which PECD has been previously reported.²⁵ The class of X-HFC₃ molecules, where X is a trivalent lanthanide ion, thus provides new opportunities to study the interplay between intrinsic chirality, arising from the handedness of the ligands themselves, and structural chirality, dependent on the arrangement of the ligands. In the present case, we have no indication that P–M isomerism was resolved during the Eu-HFC₃ synthesis, and as such the molecules studied are likely racemic in this respect. Separating isomers of organometallic complexes is possible using methods such as chiral high-performance liquid chromatography.^{59,60} However, such separation is not trivial, primarily due to the non-negligible effects that solute-solvent interactions may have on conformational stability of the molecules in question.

We note that the photoelectrons coincident with Eu-HFC₃'s parent ion comprise a similar spectrum [Fig. 2(d)] to that measured for HFC, with the notable difference being the presence of a new lower-energy feature with IE ≈ 8.2 eV. This PE feature is clearly attributable to Eu-HFC₃'s HOMO, and our calculations reveal that the corresponding electron density for this orbital is primarily delocalized across the ring defined by the Eu-binding diketonate groups of the ligands [see Fig. 5(b)]. This is different from the case of Ru(acac)₃,²⁵ for which the HOMO was strongly metal localized and reflects the lower stability of the occupied metal valence orbitals for transition metal complexes generally. The DFT calculations show that the Eu-HFC₃ HOMO is almost threefold energetically degenerate (Table S4, right column, orbitals 1–3). The Kohn-Sham HOMO and HOMO-1 [see Fig. 5(b)] differ in energy by only 0.001 eV, with HOMO-2 being only ca. 0.02 eV more stable. The molecule was optimized without symmetry constraints but is almost C₃-symmetric; in perfect C₃ symmetry, the HOMO and HOMO-1 would be the two components of an e symmetry orbital pair, with HOMO-2 being of a symmetry. This pseudo e + a orbital

and HOMO-1 of Eu-HFC₃ (Table S4), which agrees well with the measured data and supports these feature assignments. The third PE feature, centered near IE \approx 10 eV, is formed by the overlap of the HOMO-3 and HOMO-4, with more strongly bound MOs combining to form a higher-energy plateau beginning at 10.5 eV.

As mentioned earlier, the bidentate HFC binding geometry presented in Fig. 5(a) [see also Fig. 1(c)] assumes that the HFC ligands adopt an enol-like structure, with the central Eu(III) ion serving as the sixth member of a stable ring structure involving the ligand diketonate group. This structural similarity is reflected in the orbital character of Eu-HFC₃'s HOMO and HOMO-1, which more closely resemble those of enol HFC than keto HFC [compare Figs. 5(b) and 5(c) to Figs. 4(e) and 4(f)], with the HOMO delocalized across the diketonate group and the HOMO-1 more localized on the O lone pairs. Our calculated and experimentally measured ionization energies provide support for this picture. The measured VIE of the Eu-HFC₃ HOMO is more similar to the calculated values for the enol-HFC HOMO than for the keto-HFC HOMO. The VIE of the Eu-HFC₃ HOMO-1 is nearly aligned with the VIE of the keto-HFC HOMO, seemingly reflecting the orbital similarities between keto-HFC HOMO and enol-HFC HOMO-1 and strongly suggesting "locking-in" of enol-HFC structure upon coordination to Eu(III). The greater conformational landscape of Eu-HFC₃ is difficult to define, given the many possible rotations of the ligand CF₂·CF₂·CF₃ tail grouping. However, given the likely ligand packing arrangement presented in Fig. 5(a), we note that some cooperative steric stabilization of the ligand tails may be expected. In both of these cases, the PECD data could be the definitive piece of evidence. Unfortunately, PECD calculations for such large organometallic molecules remain exceptionally difficult at the moment, and their implementation here is not yet practical.

We note that the PECD measured for the HOMO and HOMO-1 of Eu-HFC₃ and HFC, when compared (Fig. 3), shares qualitative similarities in terms of sign and kinetic-energy trends. As the chirality of Eu-HFC₃ stems from the chirality of its individual HFC ligands, it may be tempting to ascribe these similarities to this shared chirality between the molecules. However, given that the HOMO and HOMO-1 of the two molecules differ substantially, and that our PES data and calculations suggest different dominant tautomers for free and coordinated HFC, this apparent consistency seems likely to be simply a coincidence. Even if the MOs were very similar, complexes of chiral molecules are generally clearly distinguishable from their monomers in terms of PECD.^{14,61,62}

V. CONCLUSIONS

We have recorded photoelectron spectra and PECD spectra for the gas-phase ligand HFC and its Eu(III) complex, Eu(HFC)₃. We utilized DFT calculations to examine the relative stabilities and ionization energies of different conformations of the free HFC molecule. Despite the considerable flexibility of the CF₂·CF₂·CF₃ tail grouping, a rather consistent picture emerges with the ionization energies of the outer orbitals, which are localized around the more rigid camphor structure, being in good agreement with the experimental PES results. The role of keto-enol tautomerism in the gas-phase HFC is discussed, with calculations indicating that the enol form is the more stable form, and so likely to be dominant in an equilibrium sample. Nevertheless, the agreement between the calculated enol HOMO ionization energy and the experimental photoelectron spectrum is worse, so that the PES evidence tends rather to support a predominance of the keto form.

One significant consequence of the keto-enol conundrum is that the keto structures are expected to be diastereomers (due to the two independent chiral centers). While cis-trans isomerism is technically possible for the enol structure across the enol double bond, our calculations indicate that the configuration with the tail hydroxyl group hydrogen bonded to the camphor carbonyl is clearly energetically preferred, meaning that enol HFC is, in practice, likely to be enantiomeric. This has obvious consequences for PECD measurements, and, in principle, the measured PECD should be well-placed to resolve keto vs enol HFC. However, such calculations near the edge of feasibility using current methods and are beyond the scope of the present paper.

For the case of Eu-HFC₃, the calculated HOMO and HOMO-1 orbitals are almost solely ligand-localized, with the Eu(III) 4f orbitals playing a minor role at most. Our lowest-energy calculated molecular structure of Eu-HFC₃ suggests that the coordinated HFC ligands adopt an enol-like structure, with the Eu(III) ion serving as one part of a stable six-membered ring involving the ligand diketonate groups. The measured PES data further support this picture. We note that the approximate C₃ symmetry of Eu-HFC₃ provides an opportunity to study the interplay between the intrinsic chirality of the individual HFC ligands and the structural P-M chirality of the complex, determined by the nature of the ligand packing. PECD would be well suited to resolve these contributions, but additional challenges remain in modeling such large molecules.

It is encouraging that the magnitude of PECD asymmetry observed for Eu-HFC₃ is comparable to that of HFC despite the differences in size and complexity between the systems. This suggests that PECD may be a viable analytical technique even for large organometallic systems. HFC is a large molecule as far as current calculations of PECD are concerned, and Eu-HFC₃ is the largest organometallic molecule for which PECD has yet been measured. The application of PECD in an analytical manner to such molecules remains challenging and will require continued advancements in approaches for modeling PECD, in particular in terms of treating multiplet structures, which might exhibit different PECD.

Our study provides a valuable addition to the presently scant literature documenting PECD in organometallic systems. We note that the class of molecules X-HFC₃, where X represents any trivalent lanthanide ion, provides ample opportunity for additional experiment. A useful subsequent study could focus on a nearly closed-shell system, such as the 4f¹ Ce-HFC₃, for which electron correlation effects are minimal, and current models might be more applicable. We note that the MO with lowest IE in this system should be Ce 4f-based, in contrast to the present Eu molecule, reflecting the gradual stabilization of the metal 4f electrons across the lanthanide series and providing a further rationale for targeting the Ce system. Moreover, we point out that X-HFC₃ molecules also provide appealing opportunities to study PECD's ability to resolve fine-structure features in PES, for example spin-orbit split states. Such application will require advances in state-of-the-art methods for modeling photoionization of relativistic electrons.⁶³ Additional experiment with this class of molecules is certainly warranted and will serve to provide useful benchmarks against which theory can be tested.

SUPPLEMENTARY MATERIAL

See the [supplementary material](#) for tabulated calculated ionization and orbital energies for HFC in both the keto (10 conformers) and enol (2 conformers) forms as well as for the optimized structure of

Eu-HFC₃. The atomic coordinates for the optimized structures of HFC (keto and enol form) and of Eu-HFC₃ are also provided.

ACKNOWLEDGMENTS

The authors acknowledge Synchrotron SOLEIL for enabling the described experiments through user proposal 20221157. V.B. acknowledges support from the International Max Planck Research School for Elementary Processes in Physical Chemistry. N.K. acknowledges the University of Manchester for access to its Computational Shared Facility and associated support services. I.P. acknowledges the University of Nottingham for the provision of computational resources on the UoN HPC cluster. D.S. acknowledges funding from the European Research Council (Grant Agreement No. 883759). This work was supported by state funding from the ANR under the France 2030 program, with reference to ANR-23-EXLU-0004, PEPR LUMA TORNADO.

AUTHOR DECLARATIONS

Conflict of Interest

The authors have no conflicts to disclose.

Author Contributions

Viktoria K. Brandt: Formal analysis (equal); Investigation (equal); Validation (lead); Visualization (equal); Writing – original draft (equal); Writing – review & editing (equal). **Michele Pugini:** Investigation (equal); Writing – review & editing (equal). **Nikolas Kaltsoyannis:** Formal analysis (equal); Methodology (equal); Visualization (equal); Writing – review & editing (equal). **Gustavo Garcia:** Investigation (equal); Methodology (equal); Software (lead); Writing – review & editing (equal). **Ivan Powis:** Conceptualization (equal); Formal analysis (equal); Methodology (equal); Supervision (equal); Visualization (equal); Writing – review & editing (lead). **Laurent Nahon:** Conceptualization (equal); Investigation (equal); Methodology (equal); Supervision (equal); Writing – review & editing (equal). **Dominik Stemer:** Conceptualization (lead); Formal analysis (equal); Investigation (equal); Project administration (lead); Visualization (equal); Writing – original draft (lead); Writing – review & editing (equal).

DATA AVAILABILITY

The data that support the findings of this study are available from the corresponding author upon reasonable request.

REFERENCES

- I. Powis, “Photoelectron circular dichroism in chiral molecules,” in *Advances in Chemical Physics*, edited by S. A. Rice (John Wiley & Sons, Inc., 2008), pp. 267–329.
- L. Nahon, G. A. Garcia, and I. Powis, “Valence shell one-photon photoelectron circular dichroism in chiral systems,” *J. Electron Spectrosc.* **204**, 322–334 (2015).
- C. Sparling and D. Townsend, “Two decades of imaging photoelectron circular dichroism: From first principles to future perspectives,” *Phys. Chem. Chem. Phys.* **27**, 2888–2907 (2025).
- B. Ritchie, “Theory of the angular distribution of photoelectrons ejected from optically active molecules and molecular negative ions,” *Phys. Rev. A* **13**, 1411–1415 (1976).
- B. Ritchie, “Theory of angular distribution for ejection of photoelectrons from optically active molecules and molecular negative ions. II,” *Phys. Rev. A* **14**, 359–362 (1976).
- N. Böwering, T. Lischke, B. Schmidtke, N. Müller, T. Khalil, and U. Heinzmann, “Asymmetry in photoelectron emission from chiral molecules induced by circularly polarized light,” *Phys. Rev. Lett.* **86**, 1187–1190 (2001).
- G. A. Garcia, L. Nahon, M. Lebeck, J.-C. Houver, D. Doweck, and I. Powis, “Circular dichroism in the photoelectron angular distribution from randomly oriented enantiomers of camphor,” *J. Chem. Phys.* **119**, 8781–8784 (2003).
- U. Hergenbahn, E. E. Rennie, O. Kugeler, S. Marburger, T. Lischke, I. Powis, and G. Garcia, “Photoelectron circular dichroism in core level ionization of randomly oriented pure enantiomers of the chiral molecule camphor,” *J. Chem. Phys.* **120**, 4553–4556 (2004).
- L. Nahon, G. A. Garcia, C. J. Harding, E. Mikajlo, and I. Powis, “Determination of chiral asymmetries in the valence photoionization of camphor enantiomers by photoelectron imaging using tunable circularly polarized light,” *J. Chem. Phys.* **125**, 114309 (2006).
- L. Nahon, L. Nag, G. A. Garcia, I. Myrgorodska, U. Meierhenrich, S. Beaulieu, V. Wanie, V. Blanchet, R. Géneaux, and I. Powis, “Determination of accurate electron chiral asymmetries in fenchone and camphor in the VUV range: Sensitivity to isomerism and enantiomeric purity,” *Phys. Chem. Chem. Phys.* **18**, 12696–12706 (2016).
- I. Powis, C. J. Harding, G. A. Garcia, and L. Nahon, “A valence photoelectron imaging investigation of chiral asymmetry in the photoionization of fenchone and camphor,” *ChemPhysChem* **9**, 475–483 (2008).
- V. Ulrich, S. Barth, S. Joshi, U. Hergenbahn, E. Mikajlo, C. J. Harding, and I. Powis, “Giant chiral asymmetry in the C 1s core level photoemission from randomly oriented fenchone enantiomers,” *J. Phys. Chem. A* **112**, 3544–3549 (2008).
- M. Stener, G. Fronzoni, D. D. Tommaso, and P. Decleva, “Density functional study on the circular dichroism of photoelectron angular distribution from chiral derivatives of oxirane,” *J. Chem. Phys.* **120**, 3284–3296 (2004).
- S. Hartweg, G. A. Garcia, D. K. Božanić, and L. Nahon, “Condensation effects on electron chiral asymmetries in the photoionization of serine: From free molecules to nanoparticles,” *J. Phys. Chem. Lett.* **12**, 2385–2393 (2021).
- J. Dupont, V. Lepère, A. Zehnacker, S. Hartweg, G. A. Garcia, and L. Nahon, “Photoelectron circular dichroism as a signature of subtle conformational changes: The case of ring inversion in 1-indanol,” *J. Phys. Chem. Lett.* **13**, 2313–2320 (2022).
- M. Stener, D. Di Tommaso, G. Fronzoni, P. Decleva, and I. Powis, “Theoretical study on the circular dichroism in core and valence photoelectron angular distributions of camphor enantiomers,” *J. Chem. Phys.* **124**, 024326 (2006).
- P. V. Demekhin, A. Ehresmann, and V. L. Sukhorukov, “Single center method: A computational tool for ionization and electronic excitation studies of molecules,” *J. Chem. Phys.* **134**, 024113 (2011).
- P. Decleva, M. Stener, and D. Toffoli, “Continuum electronic states: The Tiresias code,” *Molecules* **27**, 2026 (2022).
- R. Hadidi, D. K. Božanić, H. Ganjtabar, G. A. Garcia, I. Powis, and L. Nahon, “Conformer-dependent vacuum ultraviolet photodynamics and chiral asymmetries in pure enantiomers of gas phase proline,” *Commun. Chem.* **4**, 72 (2021).
- M. Tia, B. Cunha De Miranda, S. Daly, F. Gaie-Levrel, G. A. Garcia, L. Nahon, and I. Powis, “VUV photodynamics and chiral asymmetry in the photoionization of gas phase alanine enantiomers,” *J. Phys. Chem. A* **118**, 2765–2779 (2014).
- S. Turchini, D. Catone, G. Contini, N. Zema, S. Irrera, M. Stener, D. Di Tommaso, P. Decleva, and T. Prosperi, “Conformational effects in photoelectron circular dichroism of alaninol,” *ChemPhysChem* **10**, 1839–1846 (2009).
- S. Daly, I. Powis, G. Garcia, H. Soldi-Lose, and L. Nahon, “Photoionization of epichlorohydrin enantiomers and clusters studied with circularly polarized vacuum ultraviolet radiation,” *J. Chem. Phys.* **134**, 064306 (2011).
- D. Catone, M. Stener, P. Decleva, G. Contini, N. Zema, T. Prosperi, V. Feyer, K. C. Prince, and S. Turchini, “Resonant circular dichroism of chiral metal-organic complex,” *Phys. Rev. Lett.* **108**, 083001 (2012).
- D. Catone, S. Turchini, M. Stener, P. Decleva, G. Contini, T. Prosperi, V. Feyer, K. C. Prince, and N. Zema, “Photoelectron spectroscopy and circular dichroism of a chiral metal-organic complex,” *Rend. Lincei* **24**, 269–275 (2013).

- ²⁵B. Darquié, N. Saleh, S. K. Tokunaga, M. Srebro-Hooper, A. Ponzi, J. Autschbach, P. Declava, G. A. Garcia, J. Crassous, and L. Nahon, "Valence-shell photoelectron circular dichroism of ruthenium(III)-tris-(acetylacetonato) gas-phase enantiomers," *Phys. Chem. Chem. Phys.* **23**, 24140–24153 (2021).
- ²⁶H. C. Aspinall, "Chiral lanthanide complexes: Coordination chemistry and applications," *Chem. Rev.* **102**, 1807–1850 (2002).
- ²⁷F. Zinna, U. Giovannella, and L. D. Bari, "Highly circularly polarized electroluminescence from a chiral europium complex," *Adv. Mater.* **27**, 1791–1795 (2015).
- ²⁸S. Mayer and J. Kessler, "Experimental verification of electron optic dichroism," *Phys. Rev. Lett.* **74**, 4803–4806 (1995).
- ²⁹S. Mayer, C. Nolting, and J. Kessler, "Electron scattering from chiral molecules," *J. Phys. B* **29**, 3497–3511 (1996).
- ³⁰M. Quack, J. Stohner, and M. Willeke, "High-resolution spectroscopic studies and theory of parity violation in chiral molecules," *Annu. Rev. Phys. Chem.* **59**, 741–769 (2008).
- ³¹B. Darquié, C. Stoeffler, A. Shelkovich, C. Daussy, A. Amy-Klein, C. Chardonnet, S. Zrig, L. Guy, J. Crassous, P. Souillard, P. Asselin, T. R. Huet, P. Schwerdtfeger, R. Bast, and T. Saue, "Progress toward the first observation of parity violation in chiral molecules by high-resolution laser spectroscopy," *Chirality* **22**, 870–884 (2010).
- ³²L. Nahon, N. de Oliveira, G. Garcia, J.-F. Gil, B. Pilette, O. Marcouille, B. Lagarde, and F. Polack, "DESIRS: A state-of-the-art VUV beamline featuring high resolution and variable polarization for spectroscopy and dichroism at SOLEIL," *J. Synchrotron Rad.* **19**, 508–520 (2012).
- ³³G. A. Garcia, B. K. Cunha De Miranda, M. Tia, S. Daly, and L. Nahon, "DELICIOUS III: A multipurpose double imaging particle coincidence spectrometer for gas phase vacuum ultraviolet photodynamics studies," *Rev. Sci. Instrum.* **84**, 053112 (2013).
- ³⁴G. A. Garcia, L. Nahon, and I. Powis, "Two-dimensional charged particle image inversion using a polar basis function expansion," *Rev. Sci. Instrum.* **75**, 4989–4996 (2004).
- ³⁵M. J. Frisch, G. W. Trucks, H. B. Schlegel, G. E. Scuseria, M. A. Robb, J. R. Cheeseman, G. Scalmani, V. Barone, G. A. Petersson, H. Nakatsuji, X. Li, M. Caricato, A. V. Marenich, B. G. Janesko, R. Gomperts, B. Mennucci, H. P. Hratchian, J. V. Ortiz, A. F. Izmaylov, J. L. Sonnenberg, D. Williams-Young, F. Ding, F. Lipparini, F. Egidi, J. Goings, B. Peng, A. Petrone, T. Henderson, D. Ranasinghe, V. G. Zakrzewski, J. Gao, N. Rega, G. Zheng, W. Liang, M. Hada, M. Ehara, K. Toyota, R. Fukuda, J. Hasegawa, M. Ishida, T. Nakajima, Y. Honda, O. Kitao, H. Nakai, T. Vreven, K. Throssell, J. A. Montgomery, Jr., J. E. Peralta, F. Ogliaro, M. J. Bearpark, J. J. Heyd, E. N. Brothers, K. N. Kudin, V. N. Staroverov, T. A. Keith, R. Kobayashi, J. Normand, K. Raghavachari, A. P. Rendell, J. C. Burant, S. S. Iyengar, J. Tomasi, M. Cossi, J. M. Millam, M. Klene, C. Adamo, R. Cammi, J. W. Ochterski, R. L. Martin, K. Morokuma, O. Farkas, J. B. Foresman, and D. J. Fox, *Gaussian 16 Revision C.01* (Gaussian Inc., Wallingford CT, 2016).
- ³⁶M. Ernzerhof and G. E. Scuseria, "Assessment of the Perdew–Burke–Ernzerhof exchange–correlation functional," *J. Chem. Phys.* **110**, 5029–5036 (1999).
- ³⁷C. Adamo and V. Barone, "Toward reliable density functional methods without adjustable parameters: The PBE0 model," *J. Chem. Phys.* **110**, 6158–6170 (1999).
- ³⁸S. Grimme, J. Antony, S. Ehrlich, and H. Krieg, "A consistent and accurate *ab initio* parametrization of density functional dispersion correction (DFT-D) for the 94 elements H–Pu," *J. Chem. Phys.* **132**, 154104 (2010).
- ³⁹A. D. Becke and E. R. Johnson, "A density-functional model of the dispersion interaction," *J. Chem. Phys.* **123**, 154101 (2005).
- ⁴⁰E. R. Johnson and A. D. Becke, "A post-Hartree–Fock model of intermolecular interactions," *J. Chem. Phys.* **123**, 024101 (2005).
- ⁴¹E. R. Johnson and A. D. Becke, "A post-Hartree–Fock model of intermolecular interactions: Inclusion of higher-order corrections," *J. Chem. Phys.* **124**, 174104 (2006).
- ⁴²A. K. Wilson, T. van Mourik, and T. H. Dunning, "Gaussian basis sets for use in correlated molecular calculations. VI. Sextuple zeta correlation consistent basis sets for boron through neon," *Comput. Theor. Chem.* **388**, 339–349 (1996).
- ⁴³J. Dunning and H. Thom, "Gaussian basis sets for use in correlated molecular calculations. I. The atoms boron through neon and hydrogen," *J. Chem. Phys.* **90**, 1007–1023 (1989).
- ⁴⁴R. A. Kendall, J. Dunning, H. Thom, and R. J. Harrison, "Electron affinities of the first-row atoms revisited. Systematic basis sets and wave functions," *J. Chem. Phys.* **96**, 6796–6806 (1992).
- ⁴⁵D. E. Woon, J. Dunning, and H. Thom, "Gaussian basis sets for use in correlated molecular calculations. III. The atoms aluminum through argon," *J. Chem. Phys.* **98**, 1358–1371 (1993).
- ⁴⁶W. Kuehle, M. Dolg, H. Stoll, and H. Preuss, "Energy-adjusted pseudopotentials for the actinides. Parameter sets and test calculations for thorium and thorium monoxide," *J. Chem. Phys.* **100**, 7535–7542 (1994).
- ⁴⁷X. Cao and M. Dolg, "Segmented contraction scheme for small-core actinide pseudopotential basis sets," *Comput. Theor. Chem.* **673**, 203–209 (2004).
- ⁴⁸X. Cao, M. Dolg, and H. Stoll, "Valence basis sets for relativistic energy-consistent small-core actinide pseudopotentials," *J. Chem. Phys.* **118**, 487–496 (2003).
- ⁴⁹V. G. Zakrzewski, J. V. Ortiz, J. A. Nichols, D. Heryadi, D. L. Yeager, and J. T. Golab, "Comparison of perturbative and multiconfigurational electron propagator methods," *Int. J. Quantum Chem.* **60**, 29–36 (1996).
- ⁵⁰A. L. Dempwolff, A. C. Paul, A. M. Belogolova, A. B. Trofimov, and A. Dreuw, "Intermediate state representation approach to physical properties of molecular electron-detached states. II. Benchmarking," *J. Chem. Phys.* **152**, 024125 (2020).
- ⁵¹A. L. Dempwolff, M. Hodecker, and A. Dreuw, "Vertical ionization potential benchmark for unitary coupled-cluster and algebraic-diagrammatic construction methods," *J. Chem. Phys.* **156**, 054114 (2022).
- ⁵²E. Epifanovsky, A. T. B. Gilbert, X. Feng, J. Lee, Y. Mao, N. Mardirossian, P. Pokhilko, A. F. White, M. P. Coons, A. L. Dempwolff, Z. Gan, D. Hait, P. R. Horn, L. D. Jacobson, I. Kaliman, J. Kussmann, A. W. Lange, K. U. Lao, D. S. Levine, J. Liu, S. C. McKenzie, A. F. Morrison, K. D. Nanda, F. Plasser, D. R. Rehn, M. L. Vidal, Z.-Q. You, Y. Zhu, B. Alam, B. J. Albrecht, A. Aldossary, E. Alguire, J. H. Andersen, V. Athavale, D. Barton, K. Begam, A. Behn, N. Bellonzi, Y. A. Bernard, E. J. Berquist, H. G. A. Burton, A. Carreras, K. Carter-Fenk, R. Chakraborty, A. D. Chien, K. D. Closser, V. Cofer-Shabica, S. Dasgupta, M. de Wergifosse, J. Deng, M. Diedenhofen, H. Do, S. Ehlert, P.-T. Fang, S. Fatehi, Q. Feng, T. Friedhoff, J. Gayvert, Q. Ge, G. Gidofalvi, M. Goldey, J. Gomes, C. E. Gonzalez-Espinoza, S. Gulania, A. O. Gunina, M. W. D. Hanson-Heine, P. H. P. Harbach, A. Hauser, M. F. Herbst, M. H. Vera, M. Hodecker, Z. C. Holden, S. Houck, X. Huang, K. Hui, B. C. Huynh, M. Ivanov, A. Jasz, H. Ji, H. Jiang, B. Kaduk, S. Kähler, K. Khistyayev, J. Kim, G. Kis, P. Klunzinger, Z. Koczor-Benda, J. H. Koh, D. Kosenkov, L. Koulias, T. Kowalczyk, C. M. Krauter, K. Kue, A. Kunitsa, T. Kus, I. Ladjanski, A. Landau, K. V. Lawler, D. Lefrancois, S. Lehtola *et al.*, "Software for the frontiers of quantum chemistry: An overview of developments in the Q-Chem 5 package," *J. Chem. Phys.* **155**, 084801 (2021).
- ⁵³S. Kim, E. E. Bolton, and S. H. Bryant, "PubChem3D: Conformer ensemble accuracy," *J. Cheminform.* **5**, 1 (2013).
- ⁵⁴National Center for Biotechnology Information, see <https://pubchem.ncbi.nlm.nih.gov/compound/103970#section=3D-Conformer> for "(1R)-3-(2,2,3,3,4,4,4-heptafluoro-1-oxobutyl)-1,7,7-trimethylbicyclo(2.2.1)heptan-2-one" (2025).
- ⁵⁵The unsubstituted camphor structure already has two stereogenic centers at the C₁ and C₄ atomic sites. However, because of the rigid bicyclic ring structure, the configuration at the latter is automatically determined by that of the former. Hence the R/S character of C₄ does not vary independently of C₁, and only a single enantiomer pair results in the unsubstituted camphor.
- ⁵⁶J. Pollmann, R. Franke, and J. Hormes, "Ultraviolet photoelectron spectra of fenchone, camphor and bromocamphor," *Spectrochim. Acta A* **53**, 491–493 (1997).
- ⁵⁷C. Merten, K. J. Jalkanen, V. C. Weiss, and A. Hartwig, "Vibrational circular dichroism of 3-(trifluoroacetyl)-camphor and its interaction with chiral amines," *Chirality* **22**, 772–777 (2010).
- ⁵⁸G. M. Whitesides and D. W. Lewis, "Tris[3-(tert-butylhydroxymethylene)-d-camphorato]europium(III). A reagent for determining enantiomeric purity," *J. Am. Chem. Soc.* **92**, 6979–6980 (1970).
- ⁵⁹A. Ehnbohm, S. K. Ghosh, K. G. Lewis, and J. A. Gladysz, "Octahedral Werner complexes with substituted ethylenediamine ligands: A stereochemical primer for a historic series of compounds now emerging as a modern family of catalysts," *Chem. Soc. Rev.* **45**, 6799–6811 (2016).

- ⁶⁰Y. Yoshikawa and K. Yamasaki, "Chromatographic resolution of metal complexes on sephadex ion exchangers," *Coord. Chem. Rev.* **28**, 205–229 (1979).
- ⁶¹L. Nahon, G. A. Garcia, H. Soldi-Lose, S. Daly, and I. Powis, "Effects of dimerization on the photoelectron angular distribution parameters from chiral camphor enantiomers obtained with circularly polarized vacuum-ultraviolet radiation," *Phys. Rev. A* **82**, 032514 (2010).
- ⁶²I. Powis, S. Daly, M. Tia, B. Cunha de Miranda, G. A. Garcia, and L. Nahon, "A photoionization investigation of small, homochiral clusters of glycidol using circularly polarized radiation and velocity map electron-ion coincidence imaging," *Phys. Chem. Chem. Phys.* **16**, 467–476 (2014).
- ⁶³F. Zapata, D. Toffoli, J. M. Dahlström, E. Lindroth, P. Decleva, and F. Martin, "B-spline solution of the two-center Dirac equation in the electronic continuum for relativistic molecular photoionization," *J. Chem. Theory Comput.* **20**, 10507–10523 (2024).